LBL-2500
Preprint

PHOTODISSOCIATION OF NaBr, NaI, AND KI VAPORS AND COLLISIONAL QUENCHING OF $Na^*(3\ ^2P)$, $K^*(4\ ^2P)$, AND $K^*(5\ ^2P)$ BY FOREIGN GASES

Boyd L. Earl and Ronald R. Herm

RECEIVED
LAWRENCE
RADIATION LABORATORY

JAN 31 1974

LIBRARY AND
DOCUMENTS SECTION

December 1973

Prepared for the U. S. Atomic Energy Commission
under Contract W-7405-ENG-48

TWO-WEEK LOAN COPY

This is a Library Circulating Copy which may be borrowed for two weeks. For a personal retention copy, call Tech. Info. Division, Ext. 5545

LAWRENCE BERKELEY LABORATORY
UNIVERSITY OF CALIFORNIA
BERKELEY

LBL-2500
c.2

DISCLAIMER

This document was prepared as an account of work sponsored by the United States Government. While this document is believed to contain correct information, neither the United States Government nor any agency thereof, nor the Regents of the University of California, nor any of their employees, makes any warranty, express or implied, or assumes any legal responsibility for the accuracy, completeness, or usefulness of any information, apparatus, product, or process disclosed, or represents that its use would not infringe privately owned rights. Reference herein to any specific commercial product, process, or service by its trade name, trademark, manufacturer, or otherwise, does not necessarily constitute or imply its endorsement, recommendation, or favoring by the United States Government or any agency thereof, or the Regents of the University of California. The views and opinions of authors expressed herein do not necessarily state or reflect those of the United States Government or any agency thereof or the Regents of the University of California.

PHOTODISSOCIATION OF NaBr, NaI, AND KI VAPORS AND COLLISIONAL QUENCHING OF Na^* (3 ^2P), K^*(4 ^2P), and K^*(5 ^2P) BY FOREIGN GASES

Boyd L. Earl[†] and Ronald R. Herm

Inorganic Materials Research Division, Lawrence Berkeley Laboratory and Department of Chemistry, University of California, Berkeley, California 94720

ABSTRACT

Fluorescence from excited alkali atoms (A^*) may be produced by photodissociation of alkali halide (AX) vapor. Fluorescence efficiencies have been determined as a function of the photodissociation wavelength, λ_o, for Na^*(3 ^2P) from NaBr and for K^*(4 ^2P) and K^*(5 ^2P) from KI. Employing the Stern-Volmer relation,

---

[†]Present address: Department of Chemistry, Brooklyn College of the City University of New York, Brooklyn, New York 11210

cross sections, Q_q, for the collisional quenching of the A^* electronic excitation may be determined from the attenuation of the A^* fluorescence which is observed upon introduction of a foreign gas. Because A^* may be produced with different average speeds by varying λ_o, this method permits the determination of the dependence of Q_q on relative collision speed, g. Employing this method, Q_q was determined to decrease monotonically with increasing g for $Na^*(3\ ^2P) + Br_2$ (AX = NaBr) and $K^*(4\ ^2P) + C_2H_4$, CF_3Cl, and SO_2 (AX = KI). Moreover, values of Q_q were determined at a particular g value for $K^*(4\ ^2P) + I_2$ and $K^*(5\ ^2P) + I_2$, HCl, and DCl. Alternatively, pre-mixing the quenching gas in a large (∿100-fold) excess of Ar thermal moderator (Ar failed to quench any of these A^* levels) makes possible the measurement of Q_q for a thermal distribution in g. Thermal results (800-900°K) obtained by this method are reported for the quenching of Na^* $(3\ ^2P)$ (AX = NaI), $K^*(4\ ^2P)$, and/or $K^*(5\ ^2P)$ by N_2, CF_3Cl, H_2, H_2O, CH_3OH, CF_4, CH_4, C_2H_6, C_2H_4, and SO_2. In general, for any particular quenching gas, $Q_q(K^*(5\ ^2P)) > Q_q(Na^*(3\ ^2P)) \gtrsim Q_q(K^*(4\ ^2P))$. The difference between K^* $(5\ ^2P)$ and $K^*(4\ ^2P)$ (or $Na^*(3\ ^2P)$) is sometimes quite large; for CH_4, for example, $Q_q(K^*(5\ ^2P))/Q_q(K^*(4\ ^2P)) > 60$. For I_2, however, the trend is dramatically reversed with $Q_q(K^*(5\ ^2P))/Q_q(K^*(4\ ^2P)) = 0.2$. Effects of isotopic substitution were also examined; no difference in Q_q was measured for H_2 versus D_2, H_2O versus D_2O, C_2H_4 versus

C_2D_4, or HCl versus DCl. However, for $K^*(5\ ^2P)$, $Q_q(CH_4)/Q_q(CD_4) \approx Q_q(C_2H_6)/Q_q(C_2D_6) \approx \sqrt{2}$. All of these results are discussed in terms of the likely forces between the reactants and the possibility of a change-transfer intermediate.

Since the earliest observations by Wood, there have been many studies[1] of the gas-phase collisional quenching of the first excited ^2P configuration of alkali atoms by rare gases and simple (diatomic and triatomic) molecules. However, only a few studies[2-4] have examined the quenching of these configurations by more complex molecules, and there is very little data available on the quenching of higher energy configurations.[5-8] In our own laboratory, this prompted a program of examining the quenching of different configurations of alkali atoms by a variety of molecules in an attempt to gain further insight into the mechanisms of these quenching collisions.

Some results on quenching of $Na^*(3\ ^2P)$ were reported in Ref. 4 where we have suggested[9] that molecules be broadly divided into classes on the basis of their efficiency at quenching the first excited configuration of the alkali atoms. Molecules in Class I are very inefficient quenching agents; examples are the rare gases as well as non-reactive molecules whose lowest vacant molecular orbitals are typically strongly antibonding so that no

stable nor low-lying resonance negative ion states exist (e.g., the alkanes). Class II, consisting of unsaturated (e.g., N_2, CO_2, or C_2H_4) and potentially reactive (e.g., CF_3Cl) molecules,[10] is characterized by quenching cross sections (Q_q) comparable to or somewhat larger than "gas-kinetic" estimates. Molecules which form stable gaseous negative ions comprise Class III and are super-efficient quenchers with very large Q_q values which are understood in terms of formation of an intermediate ion-pair at very large reactant separation. We have also reported[6] that some Class I molecules are quite efficient at quenching $K^*(5\ ^2P)$. (See also Ref. 7.) Finally, this present paper concludes our exploratory study and reports on quenching of $Na^*(3\ ^2P)$, $K^*(4\ ^2P)$, and $K^*(5\ ^2P)$ by various Class I, II, and III molecules. In addition, some results are presented on isotopic substitution in Class I and II molecules.

APPARATUS AND EXPERIMENTAL PROCEDURE

Excited alkali atoms (A^*) are produced by photodissociation of alkali halide (AX) vapor, contained in a heated quartz cell, by ultraviolet radiation of wavelength λ_o. Fluorescence of A^* is monitored through an interference filter at a right angle to the ultraviolet flux and is presented as a reduced fluorescence efficiency, $R(\lambda_o)$ (defined as the ratio of the number of fluorescence events per second to the number of ultraviolet photons

incident per second). Experimentally, AX pressures[11,12] were sufficiently low that only a small fraction of the incident ultraviolet was absorbed and collisional quenching of A^* by AX was neglible; the incident ultraviolet flux was also weak, resulting in a very small steady-state A concentration and negligible imprisonment of the A^* resonance fluorescence.[11] With a constant incident ultraviolet flux and wavelength, the ratio of the reduced fluorescence efficiency observed with only AX present in the cell (R_0) to that observed after addition of a foreign gas at a number density [M] determined the rate constant, k_q, for collisional quenching of A^* by M from the Stern-Volmer relation:

$$R_0/R_{[M]} = 1 + \tau k_q[M] . \qquad (1)$$

Here, τ, the A^* radiative lifetime, was taken as[13] 1.61×10^{-8}, 2.70×10^{-8}, and 1.40×10^{-7} sec for $Na^*(3\ ^2P)$, $K^*(4\ ^2P)$, and $K^*(5\ ^2P)$ respectively.

The apparatus is described in detail in Ref.11. It is essentially the same as that described in Ref. 4 except for two modifications. One of these consisted of enclosing the entire optical train[14] described in Ref. 4 in a vacuum chamber with a liquid-nitrogen-baffled pump so as to circumvent atmospheric absorption and permit irradiation at lower wavelengths. Since blackbody radiation from the heaters surrounding the quartz cell is the dominant source of background in the fluorescence detector, this also

improved the signal-to-noise ratio by lowering the heater power requirement. This was essential to the success of the experiments with KI vapor and, indeed, the quality of the data on quenching of $K^*(4\ ^2P)$ and $K^*(5\ ^2P)$ presented here is somewhat poorer than that on $Na^*(3\ ^2P)$ reported in Ref. 4. All of the experimental checks which were performed in Ref. 4 to insure that the quenching gas did not decompose or react with the solid or gaseous AX were also applied in the experiments reported here.[11] In this regard, the mass spectrum of deuterated samples which had been used in quenching measurements were examined extra carefully to insure against any significant deterioration of isotopic purity due to possible exchange with hydrogen containing species which might have adsorbed on the walls of the gas-handling system.

By varying λ_o, the initial A^* speed distribution is varied[4] so that the dependence of k_q on relative collision speed, g, may be determined. Data of this sort are presented here for quenching of $Na^*(3\ ^2P)$ by Br_2 and of $K^*(4\ ^2P)$ by C_2H_4, CF_3Cl, and SO_2. However, it proved impractical to vary λ_o over a significant range when studying $K^*(5\ ^2P)$ because of the rapid drop in incident ultraviolet intensity with decreasing λ_o as well as the rise in ultraviolet absorption by the quenching gas. Furthermore, data were also collected for $Na^*(3\ ^2P)$ and $K^*(4\ ^2P)$ with some relatively inefficient quenchers; here,

Q_q is comparable to or less than a "gas-kinetic" cross section so that one would expect the photodissociatively produced A^* speed distribution to relax to a significant but unknown extent prior to quenching.[4] For these reasons, a procedure was developed which permitted measurement of k_q for a thermal distribution in relative collision speeds. This consisted in pre-mixing[15] a known pressure of the quenching gas with a few hundred torr of argon and admitting aliquots of this mixture to the fluorescence cell. Since argon comprised ∿ 99% of this mixture and separate experiments failed to indicate any measurable quenching of $Na^*(3\ ^2P)$, $K^*(4\ ^2P)$, or $K^*(5\ ^2P)$ by pure argon at these pressures, it served to thermalize the A^* speed distribution prior to any quenching collision. The introduction of this high pressure of argon (with or without admitted quenching agent) into the fluorescence cell produced an initial attenuation of the A^* fluorescence which is attributed to a compression of the AX vapor. The A^* fluorescence would then grow in intensity and achieve a steady level after 3 to 5 minutes; if only pure argon had been admitted, this steady level always equalled that present before admission of the gas. For this reason, this argon thermalizing procedure was not applied with H_2O, D_2O, Br_2, or I_2 because these gases were adsorbed rapidly (i.e., on a time scale of minutes) on the walls (and/or stopcock grease) of the gas-handling line. It was followed in

all other measurements of thermal k_q values except for experiments with H_2 or D_2. This thermalizing procedure was judged unnecessary for H_2, D_2, H_2O, or D_2O as quenching agents, because, irrespective of the A^* speed distribution, the distributions in relative speed of collision with these very light gases are largely determined by their thermal speed distributions.[4] This was confirmed in separate experiments on $K^*(5\ ^2P) + CH_4$ where k_q values measured with and without application of the argon thermalizing procedure were in satisfactory agreement.[6]

DATA ANALYSIS AND RESULTS

Alkali Halide Photodissociation

For $Na^*(3\ ^2P)$ and $K^*(5\ ^2P)$, fluorescence was observed through interference filters which transmitted both components of the resonance doublet. For $K^*(4\ ^2P)$, however, different interference filters were used to separate the 7665 Å and 7699 Å resonance line components. Reduced fluorescence efficiency curves for $Na^*(3\ ^2P)$ from NaI are reported in Ref. 4. Figures 1-3 show similar curves for $Na^*(3\ ^2P)$ from NaBr, $K^*(4\ ^2P_{1/2})$ and $K^*(4\ ^2P_{3/2})$ from KI, and $K^*(5\ ^2P)$ from KI. Data for Li^* $(2\ ^2P)$ from LiI which are also shown in Fig. 3 are very rough and only of qualitative significance. Although Li^* would be ideally suited for quenching studies by virtue of its light mass and simple electronic structure, the LiI vapor was observed

to rapidly attack the quartz suprasil cell windows while the data shown in Fig. 3 were being collected, and no further studies with Li salts were attempted. The curves in Figs. 1-3 have all been normalized to unit peak amplitude. The actual ratio of $K^*(4\ ^2P_{3/2})$ to $K^*(4\ ^2P_{1/2})$ produced by irradiation at 2400 Å was determined to be 2.4 ± 0.1.

Table I lists threshold wavelengths (λ_t) for photodissociation of AX, calculated from

$$\lambda_t^{-1} = T_\infty = D_o^{\circ}(AX) + E^*, \qquad (2)$$

where E^* is the excitation energy of the atomic photodissociation products. As is indicated by calculated fits to $R(\lambda_o)$ presented later in this section, the thermal vibrational excitation of AX as well as the incident ultraviolet bandwidth result in experimental threshold wavelengths ∿ 200 Å higher than the entries in Table I, although $R(\lambda_o)$ does not reach 10% of its peak value until within at least 100 Å of these values. In applying Eq. (1) to determine k_q values, we are implicitly assuming that the fluorescence which we measure from a particular A^* state is produced by excitation of AX to an excited electronic state which dissociates into this same A^* state on a time scale which is short compared with the A^* radiative lifetime. The fluorescence curves in Figs. 1-3 have shapes characteristic of such photoexcitations to

the unbounded regions of potential curves for excited AX states. For NaI and NaBr, this has been directly confirmed by pulsed photodissociation experiments reported in Ref. 16. All data on quenching of first excited configurations were collected with minimum photodissociation wavelengths of 2300, 2150, and 1875 Å for KI, NaI, and NaBr vapors, respectively, which Table I indicates precluded any possible production of higher energy alkali configurations[17] which might have contributed to the observed fluorescence via a cascade radiation process. These assignments are also in agreement with assignments of peaks in the alkali halide absorption spectra reported in Ref. 18.

All results on quenching of $K^*(5\ ^2P)$ were obtained by photodissociation of KI at 1925 Å. Again, Table I, in conjunction with the $K^*(5\ ^2P)$ fluorescence efficiency curve shown in Fig. 3, indicates that no higher energy K configuration (e.g., 4 d or 6 s) should contribute to the observed fluorescence at this photodissociation wave length. Moreover, no variation was observed[11] in the rate constant for collisional quenching of $K^*(5\ ^2P)$ by CH_4 upon photodissociation of KI at 1925, 1950, and 1975 Å. This provided an independent check that no higher energy configurations contributed to the $K^*(5\ ^2P)$ fluorescence because, if present at all, contributions due to 4 d or 6 s should have risen significantly on proceeding from 1975 Å to 1925 Å and altered the measured k_q value.

As discussed in Ref. 4, the observed A^* fluorescence may arise from excitation to two or more excited electronic states of AX so that only an average potential energy function for the excited state may be determined. This has been done for the data shown in Figs. 1 and 2 by the method described in Ref. 4 which proceeds by assuming a Rittner ionic model for the ground state AX potential function. Table I lists the ground state AX dissociation energies which were used to achieve the best fit to the data; other parameters of the ground state potential functions employed are listed in Ref. 11. With the ground state potential function fixed, various forms for the excited state potential function are assumed and vibrational wave functions and Franck-Condon (F-C) overlap integrals are evaluated numerically until, by trial and error, a good fit to the experimental data is obtained. Figures 4 and 5 show potential energy functions evaluated in this manner. The data clearly indicate that transitions take place to repulsive cores of excited state potentials, but provide no indication whether these potentials possess attractive regions at larger AX internuclear separations.

Although of no consequence to the measurements of quenching cross sections, the second region of K^* ($4\ ^2P$)

growth shown in Fig. 2 below ∿ 2200 Å might arise from either of two processes:

$$KI(X^1\Sigma^+) \rightarrow K^*(4\ ^2P) + I^*(^2P_{1/2}) \qquad \text{(I)}$$

$$\text{or} \quad KI(X^1\Sigma^+) \rightarrow K^*(5\ ^2S) + I(^2P_{3/2}). \qquad \text{(II)}$$

In agreement with the treatment of NaI in Ref. 4, the particular fit to the data shown in Fig. 2 was obtained by assuming process (I) occurred with the same electronic dipole moment matrix element and shape of the potential energy curve as for the longer wavelength dissociation process. However, an equally good fit could be obtained by assuming process (II).

Quenching Cross Sections

Figure 6 shows typical linear least-squares fits of quenching data; deviations from the unit intercept predicted by Eq. (1) which are apparent in Fig. 6 are not regarded as statistically significant. Uncertainties in k_q values which are quoted are calculated from the standard deviations in the slopes of these linear fits.

Since the $Na^*(3\ ^2P)$ and $K^*(5\ ^2P)$ fluorescences are monitored through interference filters which transmit both fine structure resonance line components, k_q values measured for either of these configurations represent averages (with respect to steady-state population

distributions) of the rate constants for quenching of the $J = 3/2$ and $1/2$ components. On the other hand, the 7665 and 7699 Å $K^*(4\ ^2P)$ resonance line components were monitored separately, and Fig. 2 illustrates that it was possible to produce a non-equilibrium ratio of the $J = 3/2$ and $1/2$ levels. Consequently, it was possible in principle to determine separate rate constants for quenching of the $J = 3/2$ and $1/2$ levels as well as that for their collisional mixing. The proper data analysis procedure is developed in Ref. 19 for an experiment wherein only one resonance line component is initially excited and the speed distributions are thermal, and Ref. 11 discusses briefly modifications of this procedure appropriate to the present experimental configuration. In practice, however, the quality of the data which was collected proved to be too poor to provide this much detailed information. Thus, for any quenching gas studied and at any KI photodissociation wavelength, data collected on either the 7665 Å or 7699 Å resonance line component could be fit to Eq. (1) to yield the same k_q within experimental error. This indicated that either (1) the rate constants were identical for quenching of the $J = 3/2$ and $1/2$ levels or (2) these levels were collisionally mixed at least as fast as they were quenched so that, again, only an average rate constant for quenching of the two levels was obtained.

Thermal Speed Distributions

The quenching cross section, Q_q (g), is related to the measured quenching rate constant by

$$k_q = \int_0^\infty Q_q(g)gP(g)dg \qquad (3)$$

where P(g) is the relative collision speed probability density distribution function. If g is thermally distributed, an "average" quenching cross section may be obtained from Eq. 3 as

$$\langle Q_q \rangle = k_q / \langle g \rangle \qquad (4)$$

where $\langle g \rangle$ is the average thermal relative collision speed, given in terms of the reduced mass of the collision pair by

$$\langle g \rangle = \left(8kT/\pi\mu\right)^{1/2} . \qquad (5)$$

Values for thermally averaged quenching cross sections which were measured in this work are listed in Table II.

Non-Thermal Speed Distributions

Using the theory developed in Ref. 4 and F-C factors computed in fitting the measured R (λ_o) curves, probability density distribution functions, $P_{\lambda_o}(V)$, for the speed of A^* produced by photodissociation of AX with a monochromator setting of λ_o were computed by convoluting the monochromator bandpass function and the thermal distributions in AX translational, rotational, and vibrational energies.

If it is assumed for purposes of an initial interpretation of the k_q measurements that Q_q is energy independent over the experimental spread in relative collision speeds and that the A^* is produced with one characteristic speed $\bar{V}$ ($\bar{V}$, the most probable A^* speed, is obtained by maximizing P_{λ_o} (V)), a phenomenological quenching cross section, $\langle Q_q \rangle$, may be calculated[4] from the measured rate constant as

$$\langle Q_q \rangle = \pi^{1/2} x k_q / \bar{v}_M \Psi(x), \tag{6}$$

where $\bar{v}_M = (2kT/M_M)^{1/2}$ is the most probable speed of the quenching gas, $x = \bar{V}/\bar{v}_M$, and

$$\Psi(x) = x\exp(-x^2) + (2x^2 + 1)\int_0^x \exp(-y^2)dy.$$

Figures 7 and 8 show $\langle Q_q \rangle$ evaluated from Eq. (6) plotted versus the characteristic relative collision speed,

$$\begin{aligned} \langle g \rangle &= \bar{V} + \bar{v}_M{}^2/3\bar{V}, \ \bar{V} > \bar{v}_M, \\ \langle g \rangle &= \bar{v}_M + \bar{V}^2/3\bar{v}_M, \bar{V} < \bar{v}_M . \end{aligned} \tag{7}$$

Figure 8 also includes results obtained for SO_2 and C_2H_4 with thermal speed distributions (taken from Table II). Strictly speaking, these results should not lie on the curves defined by the non-thermal results because of the differing speed distributions in the two types of experiments as well as the use of different measures of the characteristic collision speed. Nevertheless, the close agreement between the thermalized and non-thermalized results provides further confirmation of the reliability of the argon thermalizing procedure.

In contrast to the results for KI shown in Fig. 2, the NaBr reduced fluorescence curve shown in Fig. 1 shows no indication of the onset of a second photodissociation process at lower wavelengths, producing $Na^*(3\ ^2P) + Br^*(^2P_{1/2})$. Because the $^2P_{3/2} - {}^2P_{1/2}$ energy splitting is smaller for Br, however, the onset of this higher energy dissociation might not be detectable as a break in the reduced fluorescence efficiency curve. Table I indicates that this higher energy dissociation process might be important below $\sim$ 2000 Å. Since the data shown in Fig. 7 were analyzed assuming dissociation solely into $Na^*(3\ ^2P) + Br(^2P_{3/2})$, the $\langle Q_q \rangle$ values shown at higher $\langle g \rangle$ (notably the last two) might be somewhat too low. However, the general agreement between the $\langle Q_q \rangle$ versus $\langle g \rangle$ results for $Na^*(3\ ^2P) + Br_2$ shown in Fig. 7 and those for $Na^*(3\ ^2P) + I_2$ reported in Ref. 4 suggests that this is not a significant source of error.

As in previous studies (e.g., Refs. 4, 16, 20) of the energy dependence of the cross sections for collisional quenching of excited alkali atoms, the data shown in Figs. 7 and 8 indicate that $\langle Q_q \rangle$ drops smoothly with increasing $\langle g \rangle$. For this reason, it is convenient to assume that the true quenching cross section varies as $Q_q = K_s/g^{4/s}$ in attempting to deconvolute the experimental data. For each data point, the probability density distribution in relative collision speeds, $P_{\lambda_o}(g)$, was calculated by

numerically convoluting $P_{\lambda_o}(V)$ with the thermal distribution in quenching gas velocities. This was then employed in Eq. (3) to predict the k_q value which would be measured for a particular s and K_s, and the corresponding $\langle Q_q \rangle$ was calulated from Eq. (6) for comparison with the experimental data. As in Ref. 4, adequate fits were obtain for s in the range of 4 to 6. Figures 7 and 8 show the fits to the data which were achieved. Convolutions over $P_{\lambda_o}(g)$ produces a $\langle Q_q \rangle$ versus $\langle g \rangle$ function which exhibits a somewhat weaker speed dependence than does the true cross section. However, Ref. 4 presented comparisons of sample Q_q versus g and the corresponding $\langle Q_q \rangle$ versus $\langle g \rangle$ for $Na^*(3\ ^2P) + C_2H_4$ which illustrated that the effect of deconvoluting the experimental spread in collision speeds was small. In the present experiment, this difference was even smaller because of the use of a more representative characteristic A^* speed (the most probable value) so that the originally assumed $Q_q(g)$ functions are practically indistinguishable from the computed $\langle Q_q \rangle$ versus $\langle g \rangle$ curves shown in Figs. 7 and 8.

In addition to the data shown in Figs. 7 and 8, other results measured for non-thermal speed distributions are listed in Table III. The results on $K^*(5\ ^2P)$ were obtained by analyzing the data with a K^* speed distribution which was derived by assuming that the KI potential curve dissociating into $K^*(5\ ^2P) + I(^2P_{3/2})$ was of the same

shape as the repulsive curve shown in Fig. 4. However, this should have introduced only negligible uncertainty in the data analysis because (1) computed speed distributions are relatively insensitive to F-C factors[4] and (2) the monochromator setting of 1925 Å was near the $K^*(5\ ^2P)$ threshold, resulting in only small deviations from a thermal relative collision speed distribution (see Ref. 4). In particular, the striking qualitative behavior shown in Table III of a decrease by about a factor of five of the cross section for quenching by I_2 on proceeding from $K^*(4\ ^2P)$ to $K^*(5\ ^2P)$ is unequivocally established.

Comparison with Other Work

In Ref. 4, we noted the generally good agreement of our results on the quenching of $Na^*(3\ ^2P)$, obtained by photodissociation of NaI, with other similar studies employing NaI photodissociation as well as studies using atomic Na vapor. No previous studies have been reported for most of the quenching systems studied in this work so that only a limited comparison with the literature is possible. By photodissociating over the entire NaBr absorption region (i.e., ∿ 1900 - ∿ 2200 Å), Brus[16] reported that $\langle Q_q \rangle = 177$ Å^2 for $Na^*(3\ ^2P) + Br_2$ for $\langle g \rangle \approx 1.4$ km/sec, in excellent agreement with the data shown in Fig. 7 in

view of the very broad and poorly characterized speed distribution in his experiment.

Table IV compares the results of the present work (from Table II) with previous determinations of quenching cross sections measured with atomic alkali vapors for thermal conditions; only those results from the older literature which were judged most reliable in Lijnse's critical review[1] are included. The agreements for Na^* ($3\ ^2P$) and $K^*(4\ ^2P)$ are reasonable. Thus, the literature data on H_2 suggest a $\langle Q_q \rangle$ which decreases monotonically with increasing temperature[21] and are in good agreement with the results found here. The reasonable agreement for Na^* ($3\ ^2P$) and $K^*(4\ ^2P) + H_2O$ is gratifying because these cross sections were especially difficult to measure[29] and were regarded as the least reliable entries in Table II.

The agreement for $K^*(5\ ^2P) + N_2$ is also very good. Indeed, since the quenching cross section for this system is rather large, it might be expected to decrease with increasing temperature simply because of the changing speed distribution. If our value of 60 $Å^2$ obtained at 893°K is corrected to the speed distribution at 1900°K assuming $Q_q = K_6/g^{2/3}$, a value of 47 $Å^2$ is obtained, in excellent agreement with the result reported in Ref. 5. In contrast, however, there is a large discrepancy between our results and those reported in Ref. 5 for $K^*(5\ ^2P) + H_2$ and H_2O. Of course, the results measured here need

not agree with those reported in Ref. 5 in view of the large temperature differences. For example, very little is known about the dependence of quenching cross sections on internal state distributions of the quenching gas, although it seems unlikely that this affect could account for the differences shown in Table IV. Both experiments simply determine rate constants for the net collisional destruction of the $K^*(5\ ^2P)$ excitation. Table I indicates that $K^*(5\ ^2P)$ is bracketed by $K^*(3\ ^2D)$, 3170 cm^{-1} lower in energy, and $K^*(4\ ^2D)$, 2700 cm^{-1} higher in energy. These energy splitting are sufficiently larger than kT in the present experiment that collisional production of $K^*(4\ ^2D)$ from $K^*(5\ ^2P)$ or of $K^*(5\ ^2P)$ from $K^*(3\ ^2D)$ which had been produced in a quenching collision are negligible. Owing to the higher temperatures in Ref. 5, however, both processes could be important and could cause deviations of either sign between k_q values measured in the two experiments. Here again, however, it seems unlikely that this effect could account for the large discrepancies which are observed.

DISCUSSION

A simple model of a possible quenching collision pictures the A^* and M reactants approaching under the influence of some intermolecular potential, $V(R_{A-M})$. If

they manage to penetrate to some critical region of A-M intermolecular separation (R^*) where their initial electronic state is coupled to other final states, quenching may take place with the products separating into some other unspecified electronic configuration. This might correspond to some other molecular products produced as a result of a chemical reaction; alternatively, the alkali atom might be produced in some other electronic configuration of lower energy, with energy being conserved by some enhancement of the M internal excitation and/or the recoil energy of the two products. For class I molecules interacting with the lowest ^2P alkali configuration, it seems likely that this coupling region is located at small R_{A-M} where repulsion of A^* by M is dominant so that the collision partners are effectively excluded from this strong coupling region and Q_q is very small. For all other quenching systems examined here, however, Q_q is quite large, suggesting a coupling at larger R_{A-M} where A^*-M attraction is likely to be dominant. Thus, the results obtained for these systems are discussed in terms of some of the likely long-range reactant attractions and coupling mechanisms.

Reactant Attraction

In Ref. 4, we chose to discuss our results on quenching of $Na^*(3\ ^2P)$ by Class II molecules in terms of a picture

wherein those incoming trajectories which surmount the barrier in the effective potential, obtained by adding the centrifugal repulsion to the true long-range attractive potential, lead to quenching collisions. If the long-range attraction is assumed to be dominated by the dispersion forces so that $V(R_{A-M}) = -C_6/R_{A-M}^6 (C_6 > 0)$, this orbiting model predicts

$$Q_q(g) = (3\pi/2)\ (2C_6/E)^{1/3} \tag{8}$$

where $E = \mu g^2/2$ is the relative collision energy.

There are a large number of objections to such a simple model for the quenching cross section. For example, even if $V(R_{A-M})$ were adequately approximated solely by the dispersion forces, Eq. (8) would apply only for incident energies less than some critical E^* where the location of the orbiting barrier (R_o) reaches the critical separation for quenching, R^*. For $E > E^*$ where $R_o < R^*$, Q_q would be given by

$$Q_q(g) = \pi R^{*2}(1 - V(R^*)/E). \tag{9}$$

Barker and Weston[20] discuss their results on the quenching of $Na^*(3\ ^2P)$ by N_2 in terms of Eq. (9). Indeed, the magnitudes of C_6 and R^* for the systems studied in this paper are such that E^* is often expected to lie in the range of energies which contribute significantly to the experimentally measured k_q (via Eq. (3)) so that Eq. (8) is certainly not expected to be strictly applicable. However, Eq. (8) has

the advantage over Eq. (9) that it provides an estimate of the quenching cross section which contains no adjustable parameters because C_6 can be calculated from the Slater-Kirkwood approximation[4] and the known polarizabilities of M (literature references cited in Ref. 11) and A^*.[30] It should also be noted that (1) the limited information content of the data are unable to distinguish between the energy dependences embodied in Eqs. (8) and (9) and (2) Eqs. (8) and (9) diverge rather slowly for $E > E^*$. As as example of point (2), Eqs. (8) and (9) give equal Q_q values at $E^* = 2\ C_6/R^{*6}$ and Eq. (8) is only 51% in error (i.e., smaller than Eq. (9)) at $E = 27\ E^*$. If short-range repulsive forces are also included in $V(R_{A-M})$ so as to obtain a more realistic intermolecular potential with a well depth ε, Eq. (8) is also not strictly applicable for $E > E_c$ because the classical phenomenon of orbiting collisions is possible only for energies less than E_c; in general, the so-called critical energy E_c is of the order of ε, although its exact value depends on the precise functional form of $V(R_{A-M})$. Gislason and Sachs[31] have discussed the effects of a repulsive core on the simple quenching model embodied in Eqs. (8) and (9) and have pointed out that Eq. (8) continues to approximate the true value of Q_q (i.e., within a factor of 2) over a wide energy range ($0 < E < \sim 30\ \varepsilon$) provided that attractive forces are dominant at R^*.

A more serious objection to Eq. (8) is the use of the dispersion forces to estimate the long-range attraction which effectively assumes that a long-range perturbation expansion of $V(R_{A-M})$ is adequate for $R_{A-M} \gtrsim R^*$ and that the A^* quadrupole moment may be ignored. These assumptions cause serious concern for $Na^*(3\ ^2P)$ or $K^*(4\ ^2P)$ and would be very difficult to rationalize for $K^*(5\ ^2P)$ because of the diffuse nature of the valence orbital for this state. Nevertheless, Table V shows a comparison of Eq. (8) with experimental results presented as "quenching efficiencies", i.e. the ratio of measured k_q value to the k_q value calculated from Eq. (8). The entries in Table V illustrate that, despite all of its shortcomings, Eq. (8) may be used to calculate an upper limit to the rate constant for quenching of $Na^*(3\ ^2P)$ or $K^*(4\ ^2P)$ by Class II molecules and of $K^*(5\ ^2P)$ by any molecule. Moreover, the experimentally determined value is typically close to that predicted by Eq. (8), with the agreement generally improving with increasing complexity (and thus vibrational level density) of the quenching molecule.[32]

Coupling Mechanism - The Electron Transfer

Laidler[33] was apparently the first to suggest that the coupling mechanism responsible for the quenching of alkali atoms might involve the transfer of an electron from A^* to M during the collision to form an $A^+ - M^-$

ion-pair intermediate. The lowest order form of this model is illustrated for K^* + M in Fig. 9 which schematically depicts plots of diabatic potential functions for approach of M upon various K^* configurations (the neutral curves) and of M^- upon K^+ (the ionic curve). The neutral curves are shown flat at large separation, indicative of the relatively weak attraction between the neutral species, with a repulsive core at smaller separation (arbitratily assumed to set in at 3 Å). These neutral curves are crossed by the ionic curve which exhibits an R_{K-M}^{-1} coulombic attraction at large separation and dissociates into K^+ and M^- at an energy of

$$\Delta = I - EA, \tag{10}$$

where I is the ionization potential of K and EA is the electron affinity of M. Four ionic curves are illustrated, corresponding to some different possible values of EA. Thus, if K^* and M penetrate to

$$R^* = e^2/(\Delta - E(K^*)) \tag{11}$$

where the elastic diabatic neutral curve crosses the ionic curve, an $K^+ - M^-$ ion-pair may form and follow the ionic curve to smaller separations. Ultimately, this ion-pair would dissociate back into the initial elastic channel or into some other neutral channel due to either a crossing of the ionic curve with some lower energy neutral curve or a chemical reaction. Actually, Fig. 9 should depict

a family of curves for each curve shown, corresponding to different vibrational energies in M and M^-; detailed calculations based on this intersecting grid of neutral and ionic curves have obtained good agreement with measured cross sections for reaction[31] and quenching[31, 34] of alkali atoms. It might be unnecessary to invoke this ionic model in interpreting all of the quenching results obtained here, especially results on $K^*(5\ ^2P)$ where the close proximity of other K^* energy levels might be expected to give rise to crossings of neutral diabatic curves even in the absence of an ion-pair intermediate. Nevertheless, the ion-pair intermediate model provides a plausible correlation and interpretation of the wide variety of phenomena presented here.

Perhaps the most striking result presented here is the decrease in the cross section for quenching by I_2 on proceeding from K^* $(4\ ^2P)$ to K^* $(5\ ^2P)$, opposite to the behavior observed with any other quenching molecule. Indeed, the Q_q for $K^*(5\ ^2P) + I_2$ given in Table III is even considerably smaller than the cross section for reaction of ground state K atoms with I_2.[35] In applying the lowest-order form of the electron transfer model (Eqs.(10) and (11)), it is unclear whether one should use the adiabatic or vertical electron affinity, 2.6 and $\sim$ 1.5eV respectively for I_2.[31]

In either case, however, the contrasting $K^*(4\ ^2P)$ and $K^*(5\ ^2P) + I_2$ behaviors observed here provide an especially straightforward confirmation of the electron transfer picture because Δ is less than the $K^*(5\ ^2P)$ excitation energy. This is illustrated by the lowest ionic curve in Fig. 9, drawn for $K^+ + I_2^-$ assuming the adiabatic electron affinity, which fails to cross the $K^*(5\ ^2P) + I_2$ neutral curve. The measured $K^*(5\ ^2P) + I_2$ cross section is finite because some quenching may take place due to either some other type of mechanism or an electron transfer mechanism involving production of an I_2^- which is vibrationally or electronically excited.

The contrasting behaviors of Class I, II, and III molecules may also be rationalized by the electron transfer model. Thus, the behavior of Class I molecules in Table V suggests that their ionic curve intersects the repulsive core of the neutral curve for $K^*(4\ ^2P) + M$ but not $K^*(5\ ^2P) + M$. Arbitrarily taking 3 Å as the onset of this repulsive core, the upper two ionic curves in Fig. 9 suggest that EA is in the range of ~ -2 to ~ -4 eV for these molecules, consistent with the available information on the lowest energy resonant negative ion states of these molecules.[6] The fact that the quenching efficiencies clearly exceed unity for Class III molecules with $Na^*(3\ ^2P)$ or $K^*(4\ ^2P)$ suggests that $E \gtrsim 10\ E^*$ for these systems. Since $E^* = 2C_6/R^{*6}$ for the simple model discussed in

developing Eqs. (8) and (9), this suggests EA >~1eV, consistent with the electron affinities of the class III quenchers listed in Table V. It might also be noted that this model further suggests that ∿-2eV < EA < ∿ 0eV (the second ionic curve in Fig. 9) for Class II molecules listed in Table V in order for their quenching efficiencies to be finite for $Na^*(3\ ^2P)$ and $K^*(4\ ^2P)$ and yet not clearly exceed unity for $K^*(5\ ^2P)$. In this regard, the behavior of H_2 and D_2 is somewhat surprising since EA ∿ -2eV[36] and the quenching efficiencies shown in Table V might have been expected to show a larger increase on proceeding from $K^*(4\ ^2P)$ to $K^*(5\ ^2P)$. In view of the relatively large vibrational energy level spacings for H_2 and H_2^- (or D_2 and D_2^-) and their approximately equal R_e and ω_e values,[36,37] however, the $A^+ - H_2^-$ ion-pair intermediate might have an especially large probability of decomposing back into the original elastic channel.

The isotope effect for $K^*(5\ ^2P) + CH_4$ and C_2H_6 shown in Table II, with $Q_q(CH_4)/Q_q(CD_4) \approx Q_q(C_2H_6)/Q_q(C_2D_6) \approx \sqrt{2}$, also warrants comment. If $K^*(5\ ^2P)$ made a transition to the next lowest energy level with a simultaneous vibrational excitation of the quenching molecule, this might arise simply because the $K^*(5\ ^2P) - K^*(3\ ^2D)$ energy separation of 3170 cm^{-1} is closer to the stretching vibration of C-H (3029 and 3156 cm^{-1} in CH_4, ∿ 2900 cm^{-1}

in C_2H_6) than C-D (2143 and 2337 cm^{-1} in CD_4, $\sim$ 2100 cm^{-1} in C_2D_6).[38] If this were the explanation, however, one might have expected a similar effect in C_2H_4 versus C_2D_4 and the reverse effect for H_2 (ω_e = 4395 cm^{-1}) versus D_2 (ω_e = 3118 cm^{-1}). If quenching of the alkanes proceeded via the exoergic $K^*(5\ ^2P) + H - R \rightarrow KH + R$ chemical reaction, absolute rate theory would predict an isotope effect of $\sim \sqrt{2}$ in the limit of very high temperature, but the temperature employed here is insufficient to classically excite the C-H (or C-D) stretches.[39] In the electron transfer model calculations[31,34] employing intersecting grids of diabatic potentials, the probability of a transition between surfaces, P, depends upon the product of an interaction matrix element between the two electronic states and the F-C factor for the transition between the vibrational levels of M and M^-. Since electron attachment in the alkanes should proceed via occupation of a C-H antibonding molecular orbital, the F-C factor for the adiabatic transition should be dominated by the behavior of the vibrational wavefunctions in the non-classical region and should be larger for the C-H stretch than for the C-D stretch. Although detailed calculations would be necessary to see if this picture can provide quantitative agreement, P should be larger for the outermost surface crossings for the hydride molecule, in qualitative accord with the observed isotope effects

in CH_4 and C_2H_6.[40] No isotope effect would be expected for H_2 versus D_2 in this picture because of the comparable[36,37] R_e values in H_2 and H_2^-. It would also predict no isotope effect for quenching of $K^*(5\ ^2P)$ by HCl, H_2O, or C_2H_4 because of the large quenching efficiencies encountered with these species. Thus, even if the probability of transfer to the ion-pair intermediate is larger for the hydride species for the outermost surface crossings, the reactants encounter so many crossings during their approach that the probability of formation of the ion-pair intermediate approaches 100% for both the hydride and deuteride species. This picture does suggest an isotope effect for H_2O versus D_2O + $Na^*(3\ ^2P)$, consistent with the entries in Table II. This is not regarded as unequivocally established, however, because the $Na^*(3\ ^2P)$ + D_2O entry in Table II is especially uncertain due to a number of experimental difficulties.

ACKNOWLEDGMENT

This work was supported by the U.S. Atomic Energy Commission through the Lawrence Berkeley Laboratory. Partial support from the Committee on Research of the University of California and the Alfred P. Sloan Foundation, in the form of a 1970 - 72 fellowship for RRH, is also gratefully acknowledged.

REFERENCES

1. For a review, see: P.L. Lijnse, "Review of Literature on Quenching, Excitation and Mixing Collision Cross Sections for the First Resonance Doublets of the Alkalis." Report i-398, Fysisch Laboratorium, Rijksuniversiteit Utrecht, The Netherlands, February, 1972.
2. R.G.W. Norrish and W.M. Smith, Proc. Roy. Soc. (London) A176, 295 (1940).
3. D.J. Dowling, G.R.H. Jones, and E. Warhurst, Trans. Faraday Soc. 55, 537 (1959).
4. B.L. Earl, R.R. Herm, S.M. Lin, and C.A. Mims, J. Chem. Phys. 56, 867 (1972).
5. H.P. Hooymayers and P.L. Lijnse, J. Quant. Spectros. Radiat. Transfer 9, 995 (1969).
6. B.L. Earl and R.R. Herm, Chem. Phys. Letters 22, 95 (1973).
7. I.N. Siara & L. Krause, Can. J. Phys. 51, 257 (1973).
8. M. Czajkowski, L. Krause, and G.M. Skardis, Can. J. Phys. 51, 1582 (1973).
9. Such broad general divisions have also been suggested previously (e.g., Ref. 2).
10. Reference 4 actually subdivided class II into unsaturated and potentially reactive molecules, but this distinction is irrelevant here.
11. B.L. Earl, Ph.D. thesis, University of California, Berkeley, 1973.

12. Temperatures quoted in the paper refer to the vicinity of the optical windows of the quartz cell and determine the energy distributions. As discussed in Ref. 4, the AX solid in the bottom of the quartz cell was maintained at a somewhat lower temperature (the salt temperature) which determined the AX pressure.

13. W.L. Weise, M.W. Smith, and B.M. Miles, Atomic Transition Probabilities. Vol. II. Nat. Stand. Ref. Data Ser., Nat. Bur. Stand. (U.S.) 22, 1964.

14. A monochromator bandpass of 60 Å (FWHM) was employed in all experiments described here.

15. Mixing was accomplished in a five liter bulb by means of a magnetically coupled fan. Absorbance measurements on SO_2 at 2100 Å reported in Ref. 11 confirmed that this produced a homogeneous mixture of known composition.

16. L.E. Brus, J. Chem. Phys. 52, 1716 (1970).

17. Actually estimates provided by Table I would not totally exclude possible Na^* ($4\ ^2S$) production from NaBr. However, this state would have to decay via cascade radiation through the $Na^*(3\ ^2P)$ intermediate level, and the NaBr fluorescence curve in Fig. 1 shows no indication of onset of such a process towards lower wavelengths.

18. P.Davidovits and D.C. Brodhead, J. Chem. Phys. 46, 2968 (1967).

19. D.A. McGillis and L. Krause, Phys. Rev. 153, 44 (1967).

20. J.R. Barker and R.E. Weston, Jr., Chem. Phys. Letters 19, 235 (1973).

21. P.L. Lijnse and Cj. Van der Maas, J. Quant. Spectros. Radiat. Transfer 13, 741 (1973).

22. D.R. Jenkins, Proc. Roy. Soc. A293, 493 (1966).

23. C. Bästlein, G. Baumgartner, and B. Brosa, Z. Phys. 218, 319 (1969).

24. B.P. Kibble, G. Copley, and L. Krause, Phys. Rev. 159, 11 (1967).

25. P.L. Lijnse and R.J. Elsenaar, J. Quant. Spectros. Radiat. Transfer 12, 1115 (1972).

26. P.L. Lijnse and J.C. Hornman, J. Quant. Spectros. Radiat. Transfer (to be published).

27. D.R. Jenkins, Proc. Roy. Soc. A303, 453 (1968).

28. G. Copley and L. Krause, Can. J. Phys. 47, 533 (1969).

29. This was due to a combination of three factors: (1) the small $\langle Q_q \rangle$ values for $Na^*(3\ ^2P)$ and $K^*(4\ ^2P)$ + H_2O; (2) the tendency of water vapor to adsorb on the walls of the gas-handling line; and (3) the tendency of water vapor at very low pressure to actually somewhat enhance the observed fluorescence intensity.

30. R.W. Schmieder, A. Lurio, and W. Happer, Phys. Rev. A3, 1209 (1971).

31. E.A. Gislason and J.G. Sachs, "Multiple-Crossing Electron-Jump Model for Reactions of Metal Atoms with Diatomic Halogen Molecules", J. Chem. Phys. (to be published).

32. L.G. Piper, J.E. Velazco, and D.W. Setser, J. Chem. Phys. 59, 3323 (1973) have pointed out that this dispersion force-orbiting model is of little use in correlating cross sections for collisional quenching of metastable rare gas atoms. This difference in behaviors might be due to a somewhat stronger coupling mechanism for the alkali collisions.

33. K.J. Laidler, J. Chem. Phys. 10, 34 (1942).

34. E. Bauer, E.R. Fischer, and F.R. Gilmore, J. Chem. Phys. 51, 4173 (1969); E.R. Fischer and G.K. Smith, Applied Opt. 10, 1803 (1971); Chem. Phys. Letters 13, 448 (1972).

35. S.A. Edelstein and P. Davidovits, J. Chem. Phys. 55, 5164 (1971).

36. I. Eliezer, H.S. Taylor, and J.K. Williams, Jr., J. Chem. Phys. 47, 2165 (1967).

37. Calculations reported in Ref. 36 indicate approximately equal R_e and ω_e for the ground states of H_2 and H_2^-, precisely the behavior required to interpret cross sections for **quenching** by H_2 or D_2 measured here in terms of the electron transfer model. It should be noted, however, that R.W. Anderson, V. Aquilanti, and D.R.

Herschbach, Chem. Phys. Letters 4, 5 (1969) interpret their measurements on collisional excitation of K by H_2 to imply a significant increase in R_e on going to the H_2^- intermediate.

38. For example, resonance (with a harmonic of the rotational frequency) has been shown to account for the temperature dependent isotope effect observed for $Cs^*(6\ ^2P_{3/2}) + CH_4 \rightarrow Cs^*(6\ ^2P_{1/2}) + CH_4$; see: W.E. Baylis, E. Walentynowicz, R.A. Phaneuf, and L. Krause, Phys. Rev. Letters 31, 741 (1973).

39. This does not exclude the possibility that CH_4 (or C_2H_6) quenching might proceed via the $K^*(5\ ^2P) + CH_4 \rightarrow KH + CH_3$ reaction. In an effort to further investigate this possibility, quenching studies were conducted with a CH_4/CD_4 sample. Subsequent mass spectral analysis showed the presence of CH_3D and CD_3H which might be formed by methyl radicals. Unfortunately, this failed to confirm quenching by reaction because this same isotopic scrambling could also be produced by irradiation at longer wave lengths where the KI did not produce $K^*(5\ ^2P)$; methyl radicals presumably formed in this case because of production of $I^*(^2P_{1/2})$.

40. The observed $K^*(5\ ^2P) + CH_4$ or C_2H_6 isotope effect might well arise due to such a dependence of curve crossing probability on F-C factor even if an ion-pair intermediate is not involved.

TABLE I. Calculated thresholds for photodissociation of alkali halide (AX) vapor.[a]

AX	Products A	Products X	E^* (cm^{-1})	threshold wavelength (λ_t) (Å)
NaI	$3\ ^2P$	$^2P_{3/2}$	16960	2360
(25300)	$3\ ^2P$	$^2P_{1/2}$	24560	2000
	$4\ ^2S$	$^2P_{3/2}$	25740	1960
NaBr	$3\ ^2P$	$^2P_{3/2}$	16960	2120
(30100)	$3\ ^2P$	$^2P_{1/2}$	20650	1970
	$4\ ^2S$	$^2P_{3/2}$	25740	1790
KI	$4\ ^2P$	$^2P_{3/2}$	12990	2500
(27000)	$4\ ^2P$	$^2P_{1/2}$	20590	2100
	$5\ ^2S$	$^2P_{3/2}$	21030	2080
	$3\ ^2D$	$^2P_{3/2}$	21530	2060
	$5\ ^2P$	$^2P_{3/2}$	24700	1930
	$4\ ^2D$	$^2P_{3/2}$	27400	1840
	$6\ ^2S$	$^2P_{3/2}$	27500	1830

[a] Numbers in parenthesis under AX column give D_0^0 (AX) in cm^{-1}; E^* is excitation energy of the atoms produced.

Table II. Quenching cross sections measured for thermal speed distributions.[a]

Quenching Gas	Excited Alkali Configuration		
	$Na^*(3\ ^2P)$	$K^*(4\ ^2P)$	$K^*(5\ ^2P)$
N_2	-	-	60 ± 5
CF_3Cl	-	-	170 ± 30
H_2	10 ± 0.4	3 ± 0.3	12 ± 0.9
D_2	8 ± 0.4	3 ± 0.3	11 ± 0.9
H_2O	3 ± 0.8	2 ± 0.7	84 ± 8
D_2O	<1	-	91 ± 8
CH_3OH	25 ± 0.9	24 ± 2	110 ± 20
CF_4	<1	<1	25 ± 5
CH_4	<1	<1	60 ± 5
CD_4	-	-	40 ± 4
C_2H_6	<1	-	98 ± 5
C_2D_6	-	-	70 ± 7
C_2H_4	-	51 ± 10	77 ± 9
C_2D_4	-	-	79 ± 10
SO_2	-	140 ± 25	-

[a]Quenching cross sections were calculated from Eq. (4) and are quoted in $Å^2$. Results on $Na^*(3\ ^2P)$ were obtained by photodissociation of NaI vapor; temperature was 820°K for H_2O and D_2O, 873°K for other gases. Results on $K^*(4\ ^2P)$ and $K^*(5\ ^2P)$ were obtained by photodissociation of KI vapor; temperature was 873°K for $K^*(4\ ^2P) + C_2H_4$, 893°K for all other measurements.

Table III. Quenching cross sections measured for non-thermal speed distributions.[a]

Collision partners	Monochromator setting (Å)	$\langle g \rangle$ (km/sec)	$\langle Q_q \rangle$ (Å^2)	10^{11} K_6 (exp) cm^2-(cm/sec)$^{2/3}$
$K^*(4\ ^2P) + I_2$	2450	0.97	210 ± 20	4.6
$K^*(5\ ^2P) + I_2$	1925	0.90	43 ± 4	0.87
$K^*(5\ ^2P) + HCl$	1925	1.0	100 ± 5	2.4
$K^*(5\ ^2P) + DCl$	1925	1.0	100 ± 5	2.4

[a]Results were obtained by photodissociation of KI vapor at 893°K; $\langle Q_q \rangle$ and $\langle g \rangle$ were calculated from Eqs. (6) and (7). The K_6 (exp) values were derived by convoluting a $Q_q(g) = K_6/g^{2/3}$ with the theoretically computed $P_{\lambda_o}(g)$ by means of Eq. (3) in order to reproduce the experimentally measured k_q.

TABLE IV. Comparison with literature of quenching cross sections measured for thermal speed distributions.[a]

Collision partners	Ref.	Literature result T	Literature result $\langle Q_q \rangle$	$\langle Q_q \rangle$ This work
$Na^*(3\ ^2P) + H_2$	21	2500	6.8 ± 1.0	8 ± 0.4
	5	1900	8 ± 1	
	27	1600-1800	9 ± 0.3	
	21	1500	9.3 ± 1.0	
	23	573	12 ± 0.7	
	24	400	16 ± 0.3	
$Na^*(3\ ^2P) + D_2$	23	573	10 ± 0.8	8 ± 0.4
	24	400	10 ± 0.3	
$Na^*(3\ ^2P) + H_2O$	5	2100	2.2 ± 0.3	3 ± 0.8
	22	1600-1800	1.6 ± 1	
	25	1750	2.2 ± 0.3	
$K^*(4\ ^2P) + H_2$	26	1500-2500	3.3 ± 0.5	3 ± 0.3
	5	1900	3.4 ± 0.3	
	27	1400-1800	3.2 ± 0.2	
	28	353	9.4 ± 1.3	
$K^*(4\ ^2P) + D_2$	28	353	8.0 ± 2.0	3 ± 0.3
$K^*(4\ ^2P) + H_2O$	26	1500-2500	3.7 ± 0.2	2 ± 0.7
	5	2100	2.6 ± 0.3	
	27	1400-1800	2.8 ± 0.9	
$K^*(5\ ^2P) + N_2$	5	1900	48 ± 10	60 ± 5
$K^*(5\ ^2P) + H_2$	5	1900	60 ± 10	12 ± 0.9
$K^*(5\ ^2P) + H_2O$	5	2100	10 ± 4	84 ± 8

a Temperatures are quoted in °K and cross sections in $Å^2$; $\langle Q_q \rangle$ from this work is taken from Table II.

Table V. Quenching efficiencies.[a]

	$Na^*(3\ ^2P)$	$K^*(4\ ^2P)$	$K^*(5\ ^2P)$
		Class I	
CH_4	<0.01	<0.01	0.45
CD_4			0.30
C_2H_6	<0.01		0.58
C_2D_6			0.41
CF_4	<0.01	<0.01	0.16
H_2O	∿0.04	∿0.03	0.71
D_2O			0.77
		Class II	
H_2	0.18	0.05	0.13
D_2	0.14	0.05	0.11
N_2	∿0.2[b]	∿0.2[b]	0.48
HCl	∿0.8[b]		0.80
DCl			0.80
CO_2	0.80	∿0.7[b]	
CH_3OH	0.26	0.24	0.74
CF_3Cl	1.0	0.82	1.0
CH_3CN	0.96		
C_2H_4	0.68	0.56	0.49
C_2D_4			0.50
C_6H_6	0.83		
		Class III	
SO_2	1.5	1.3	
Br_2	2.0		
I_2	2.2	1.8	0.22

Table V. (continued)

[a]The "quenching efficiency" is defined as the ratio of the measured k_q value (taken from this work except where noted) to that calculated from Eq. (8). The C_6 coefficients were calculated from the Slater-Kirkwood approximation using literature values for the polarizabilities of A^* (Ref. 30) and M (cited in Ref. 11).

[b]These are based on measurements of other workers using the AX photodissociation technique and have not been corrected for the experimental spread in collision speeds: $Na^*(3\ ^2P) + N_2$, Ref. 20; $K^*(4\ ^2P) + N_2$ and CO_2, J. Gatzke, Z. Physik. Chem. (Leipzig) 223, 321 (1963); $Na^*(3\ ^2P) + HCl$, H. G. Hanson, J. Chem. Phys. 23, 1391 (1955).

FIGURE CAPTIONS

Fig. 1. Data points show measured reduced fluorescence efficiency curve, $R(\lambda_o)$, (arbitrarily normalized) for $Na^*(3\ ^2P)$ from NaBr: 903°K window temperature, 883°K salt temperature. (Data below 1850 Å may not be quantitatively reliable.[11]). Solid curve shows fit to the data obtained by convoluting triangular monochromator bandpass function (60 Å FWHM) with the theoretical curve (shown dashed) calculated for the potential energy functions shown in Fig. 4.

Fig. 2. Data points show measured reduced fluorescence efficiency curves for $K^*(4\ ^2P_{1/2})$ (7699 Å) and $K^*(4\ ^2P_{3/2})$ (7665 Å) from KI: 873°K window temperature, 853°K salt temperature. Solid curves show corresponding fits to the data provided by potential energy functions shown in Fig. 5; the 7699 Å fit is also shown in the lower panel as the dashed curve for comparison to the 7665 Å fit.

Fig. 3. Data points show measured reduced fluorescence efficiency curves for $K^*(5\ ^2P)$ from KI (893°K window temperature; 873°K salt temperature) and Li^* $(2\ ^2P)$ from LiI. The Li^* data is of poor quality and is only qualitatively significant.

Fig. 4. Potential energy functions for NaBr which fit the data of Fig. 1. Also shown are the energies and

thermal populations of the vibrational levels of the ground state which were included in fitting the data of Fig. 1.

Fig. 5. Potential energy functions for KI which fit the data of Fig. 2; conventions as for Fig. 4.

Fig. 6. Least-squares fits of typical quenching data to the Stern-Volmer relation, Eq. (1). The Na^* ($3\ ^2P$) (from NaBr) + Br_2 and K^*($4\ ^2P$) (from KI) + C_2H_4 data were collected for various monochromator settings and thus changing relative collision speed distributions. Data for K^*($5\ ^2P$) were obtained by photodissociation of KI at 1925 Å; the argon thermalizing procedure was employed in collecting the CH_4 and CD_4 data.

Fig. 7. Data points show cross sections for quenching of Na^*($3\ ^2P$) by Br_2 obtained from Eqs. (6) and (7) and k_q values determined by photodissociation of NaBr at (in order of increasing speeds) 2125, 2075, 2000, 1925, and 1875 Å. The solid (s = 4), dashed (s = 5), and dotted (s = 6) curves shows the fits to the data provided by cross sections assumed to vary as $Q_q = K_s/g^{4/s}$ for K_4, K_5, and K_6 values of (units are $cm^2 - (cm/sec)^{4/s}$) 2.9×10^{-9}, 2.5×10^{-10}, and 5.0×10^{-11}, respectively.

Fig. 8. Data points show cross sections for quenching of K^*($4\ ^2P$) by SO_2, CF_3Cl, and C_2H_4 versus relative

collision speed. For SO_2 and C_2H_4, the solid point was determined from Eqs. (4) and (5) and k_q values measured for a thermal speed distribution; all other points were calculated from Eqs. (6) and (7) and k_q values measured for non-thermal speed distributions produced by photodissociation of KI at (in order of increasing $< g >$)2525, 2450, 2375, and 2300 Å. Temperatures were 893°K for SO_2 and CF_3Cl, 873°K for all C_2H_4 points except the half-darkened point obtained at 913°K. As in Fig. 7, the solid (s = 4), dashed (s = 5), and dotted (s = 6) curves show fits to the (open symbol) data for K_4, K_5, and K_6 values, respectively, as follows: 1.3×10^{-9}, 1.3×10^{-10}, and 2.8×10^{-11} for SO_2; 8.7×10^{-10}, 8.6×10^{-11}, and 1.8×10^{-11} for CF_3Cl; and 6.9×10^{-10}, 6.5×10^{-11}, and 1.3×10^{-11} for C_2H_4.

Fig. 9. Schematic diabatic potential energy diagram for approach of M upon various potassium configurations. Also shown are diabatic curves for approach of the ion-pair, drawn for four different assumed electron affinities of M. Numbers in parenthesis give asymptotic dissociation energies.

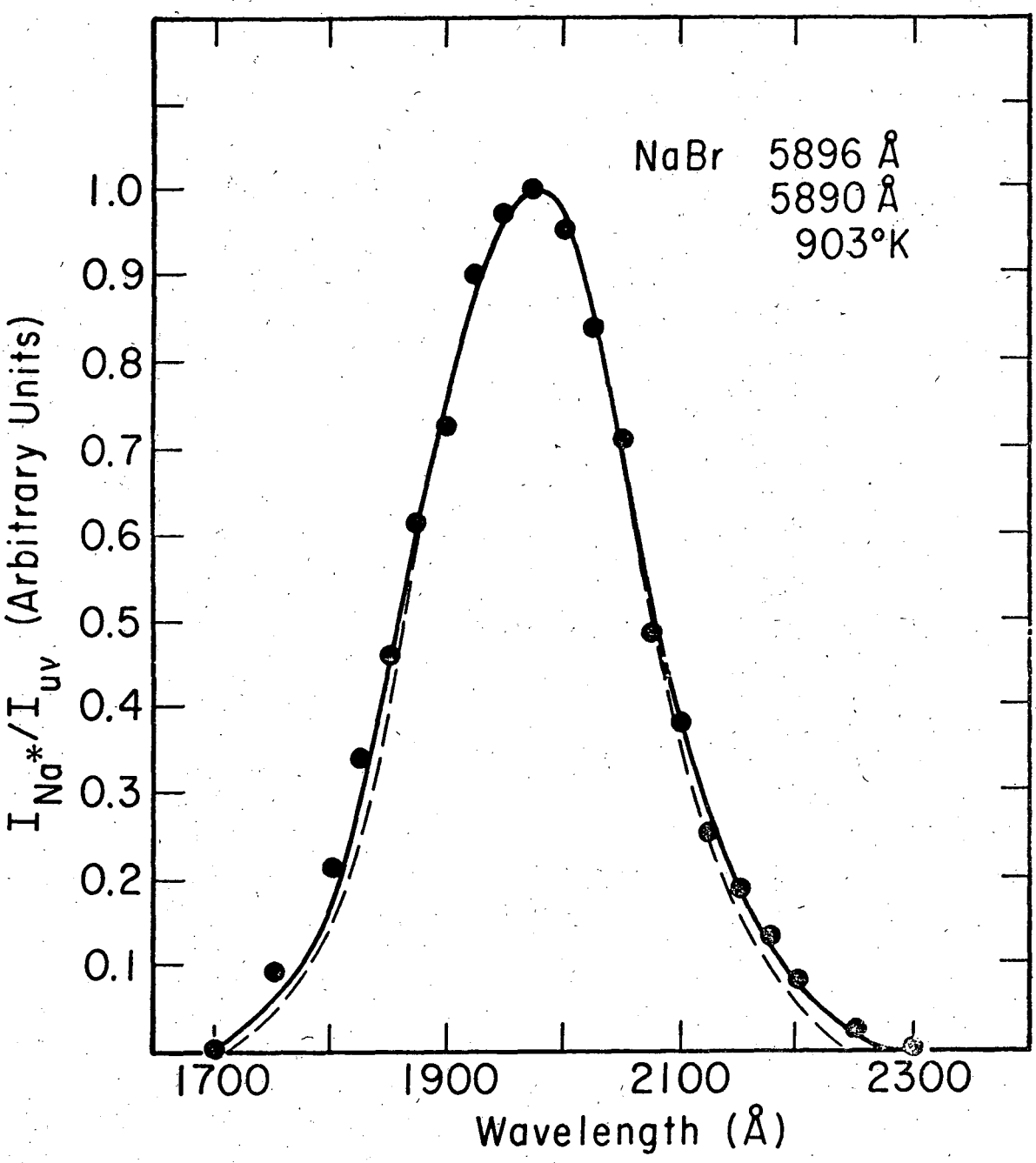

XBL 737-6562a

Fig. 1

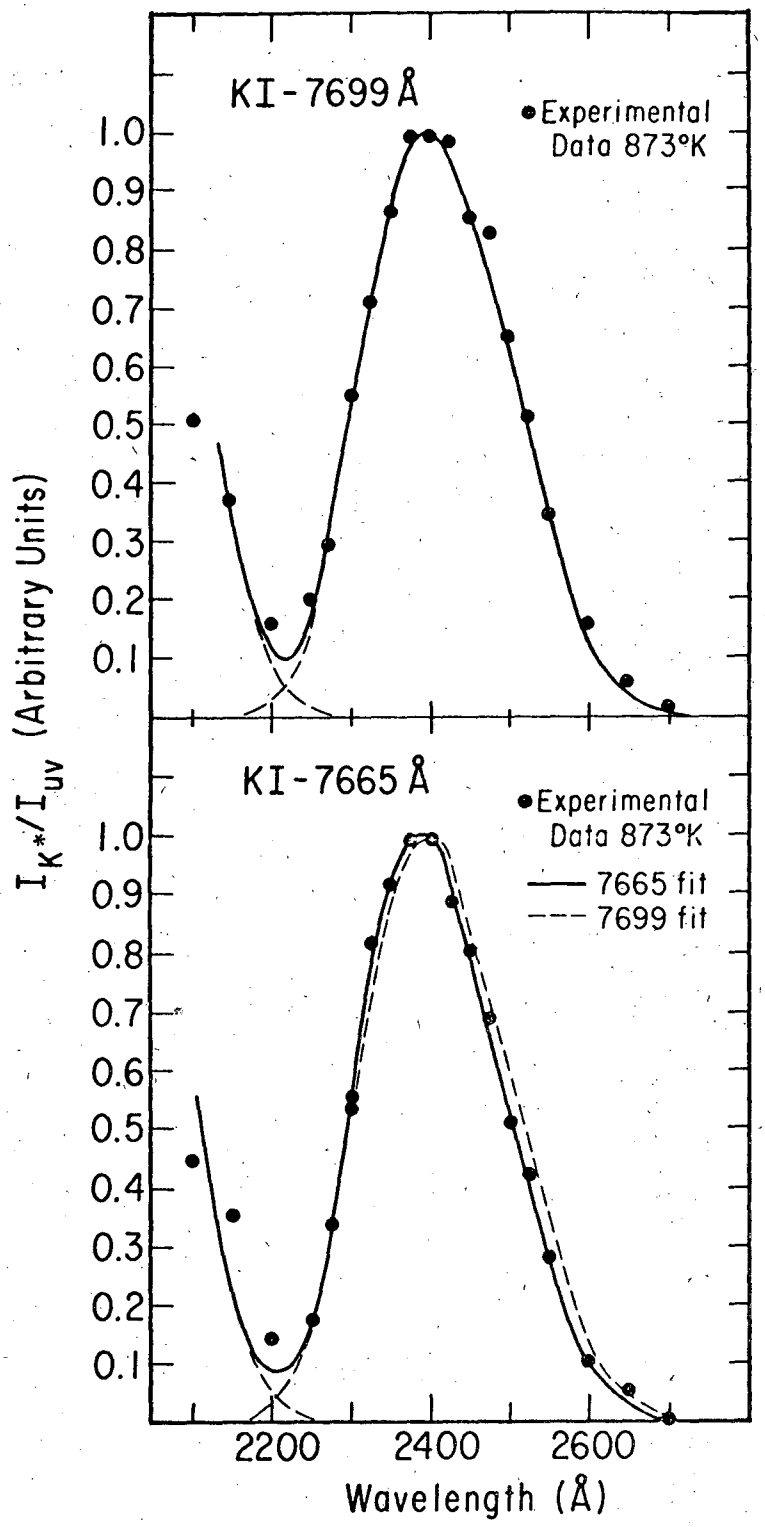

XBL 737-6567a

Fig. 2

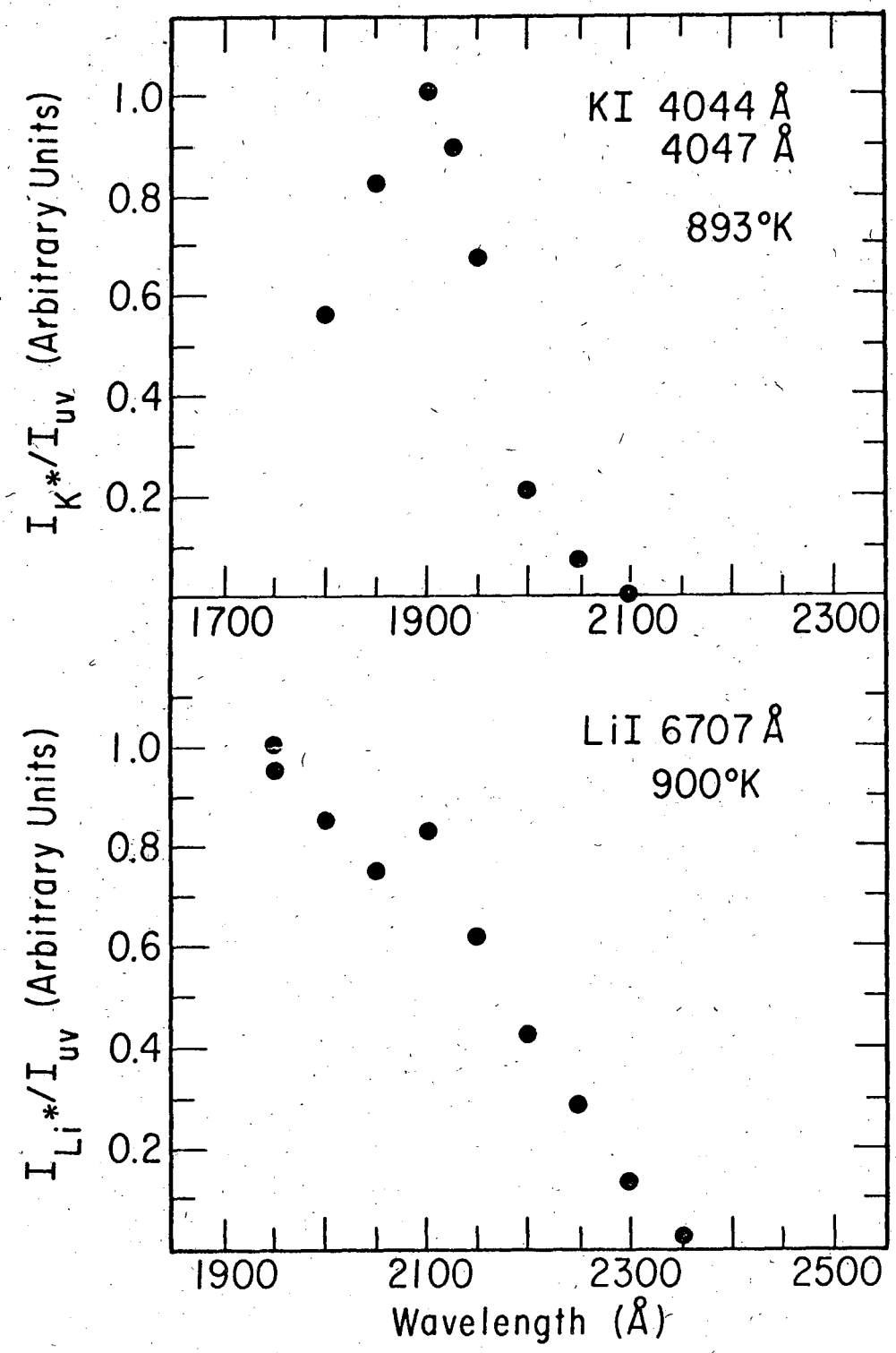

XBL 737-6565

Fig. 3

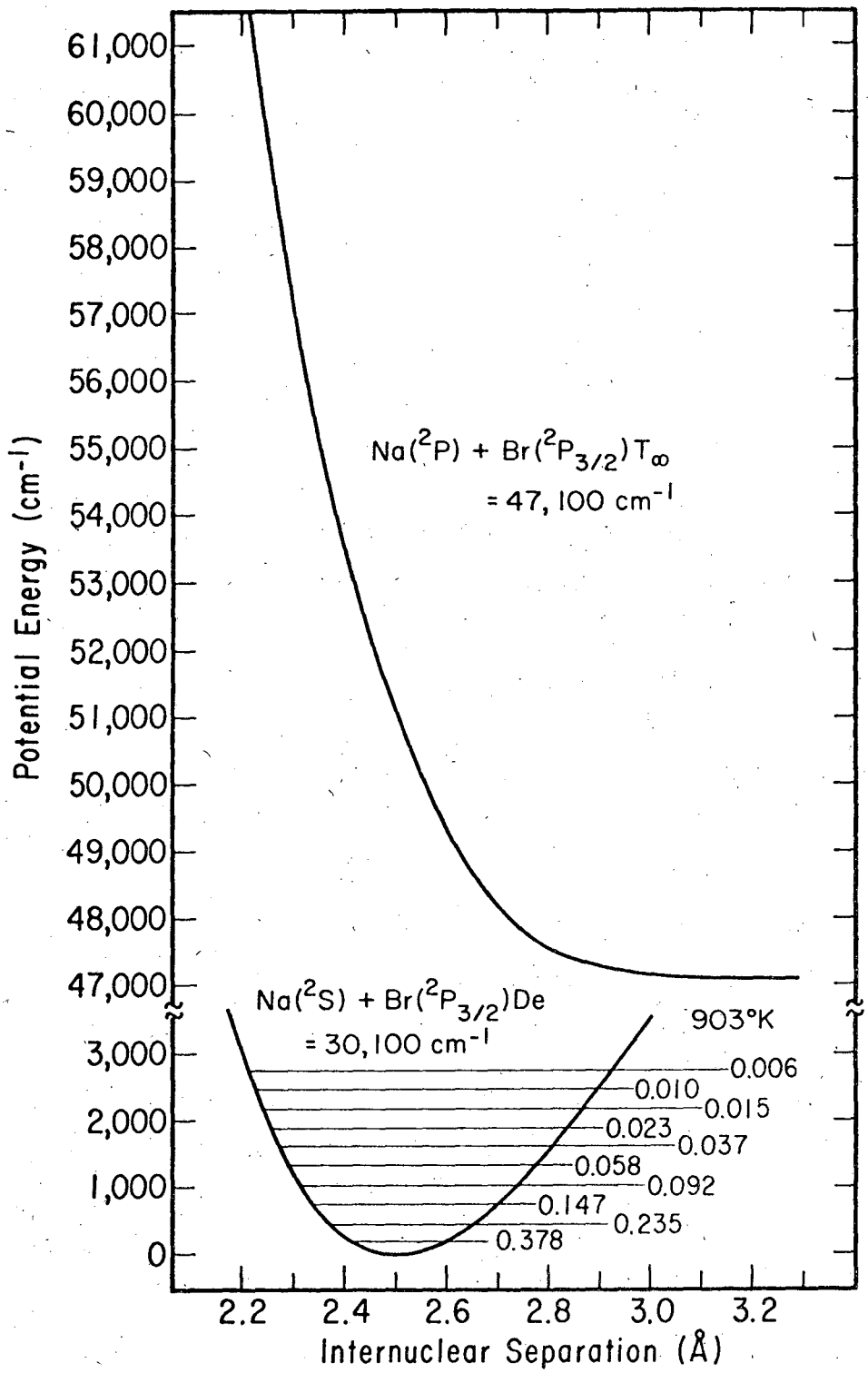

XBL 737-6564

Fig. 4

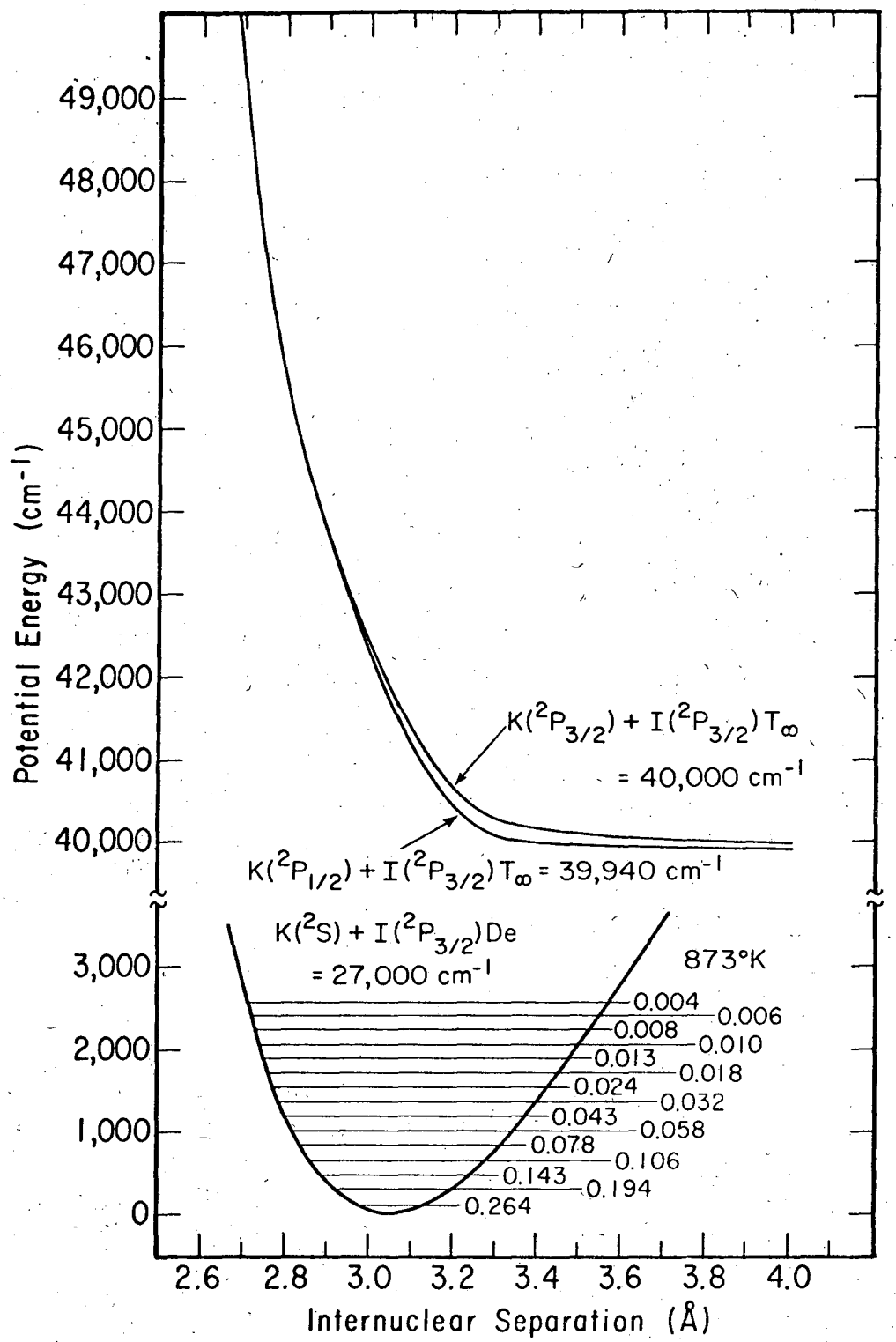

XBL 737-6566a

Fig. 5

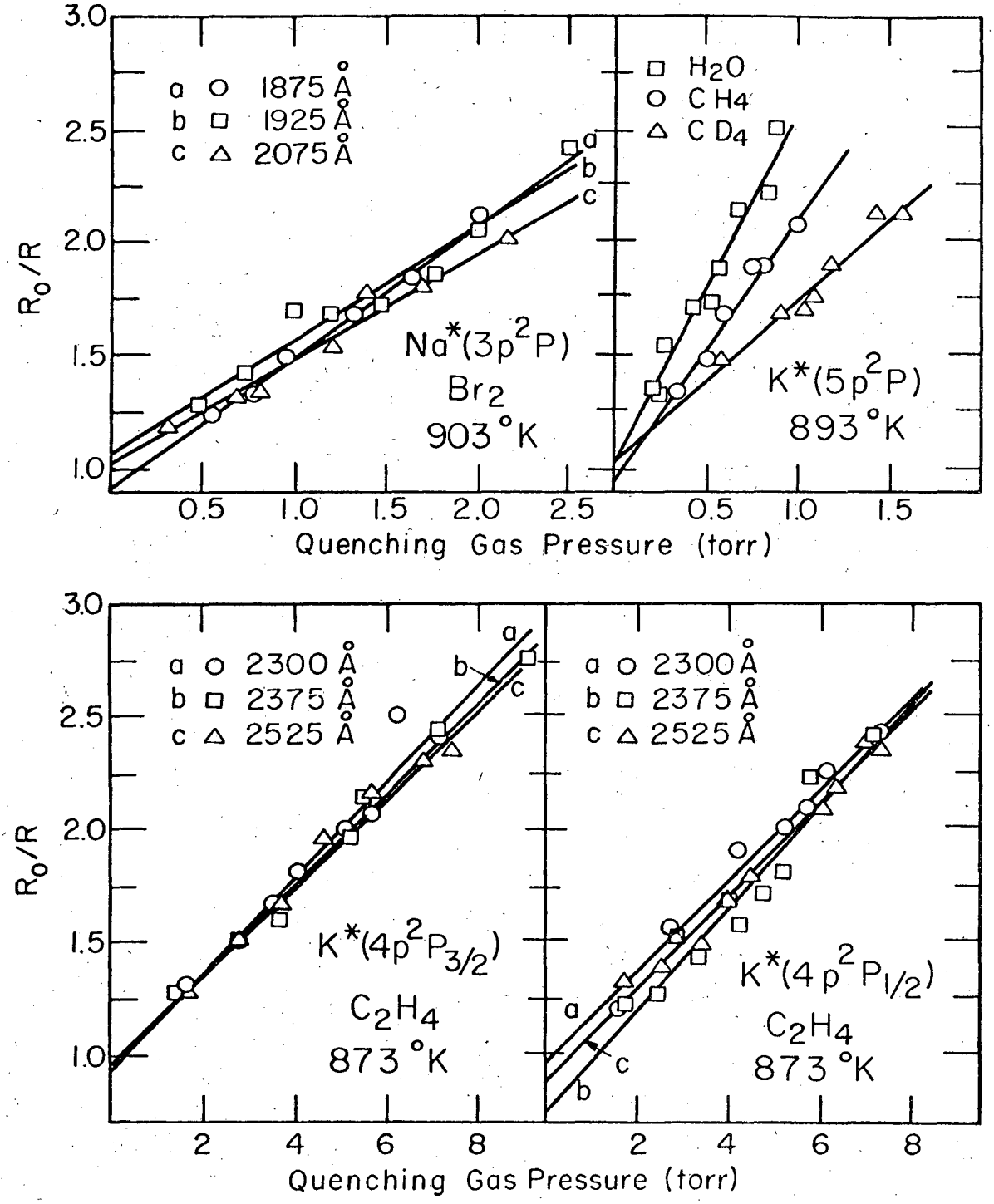

XBL738-1658a

Fig. 6

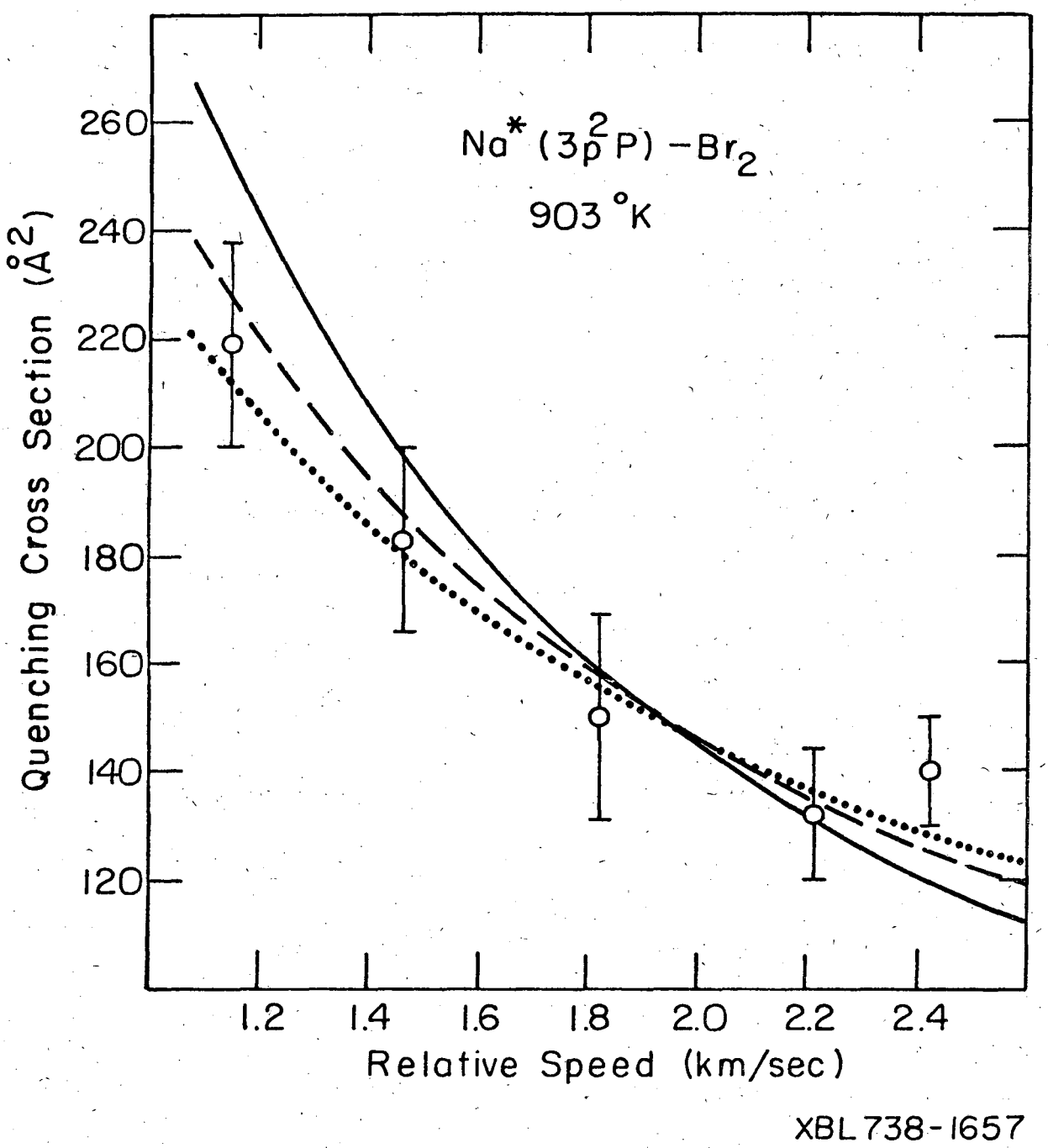

XBL 738-1657

Fig. 7

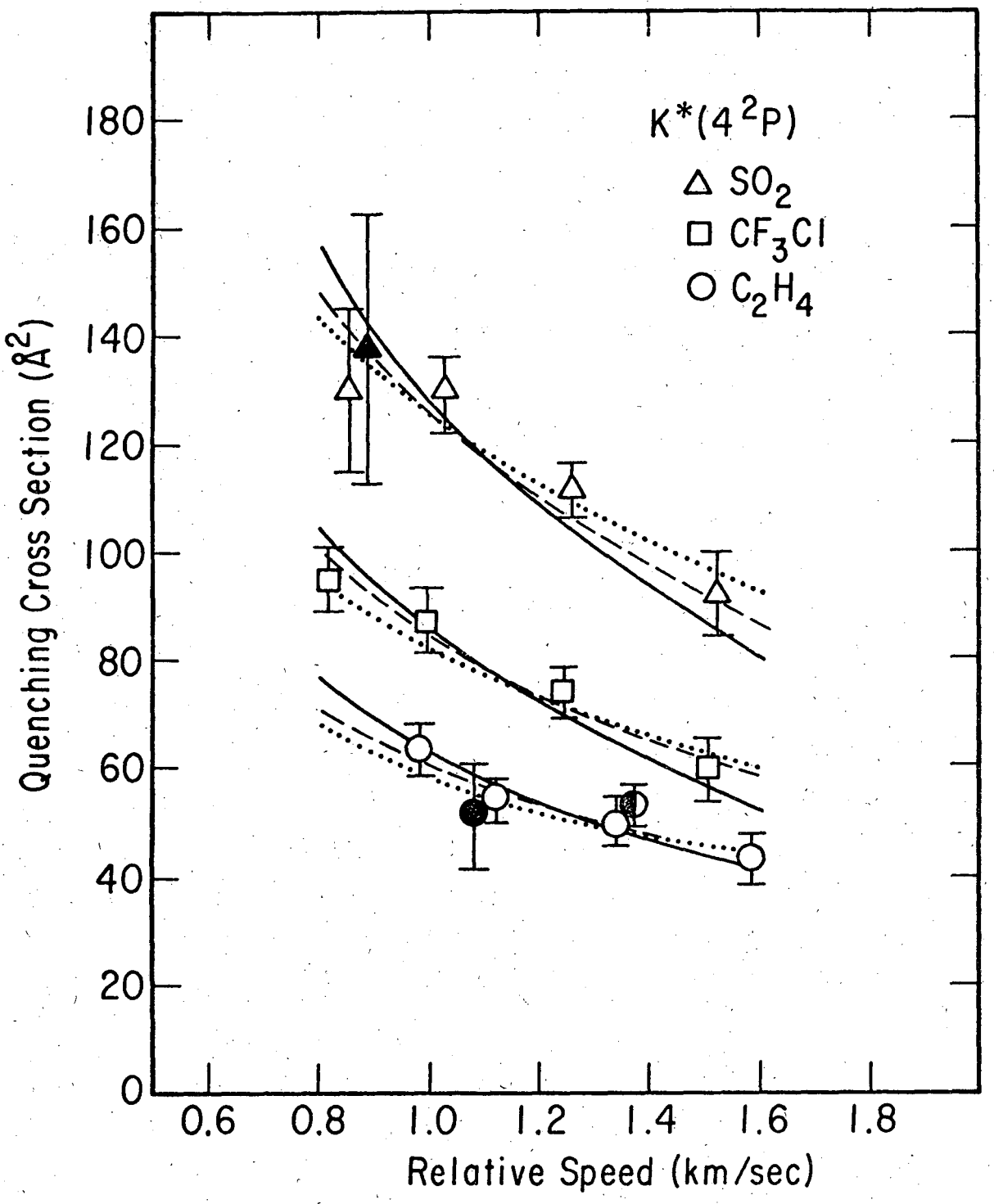

XBL 7310-1952

Fig. 8

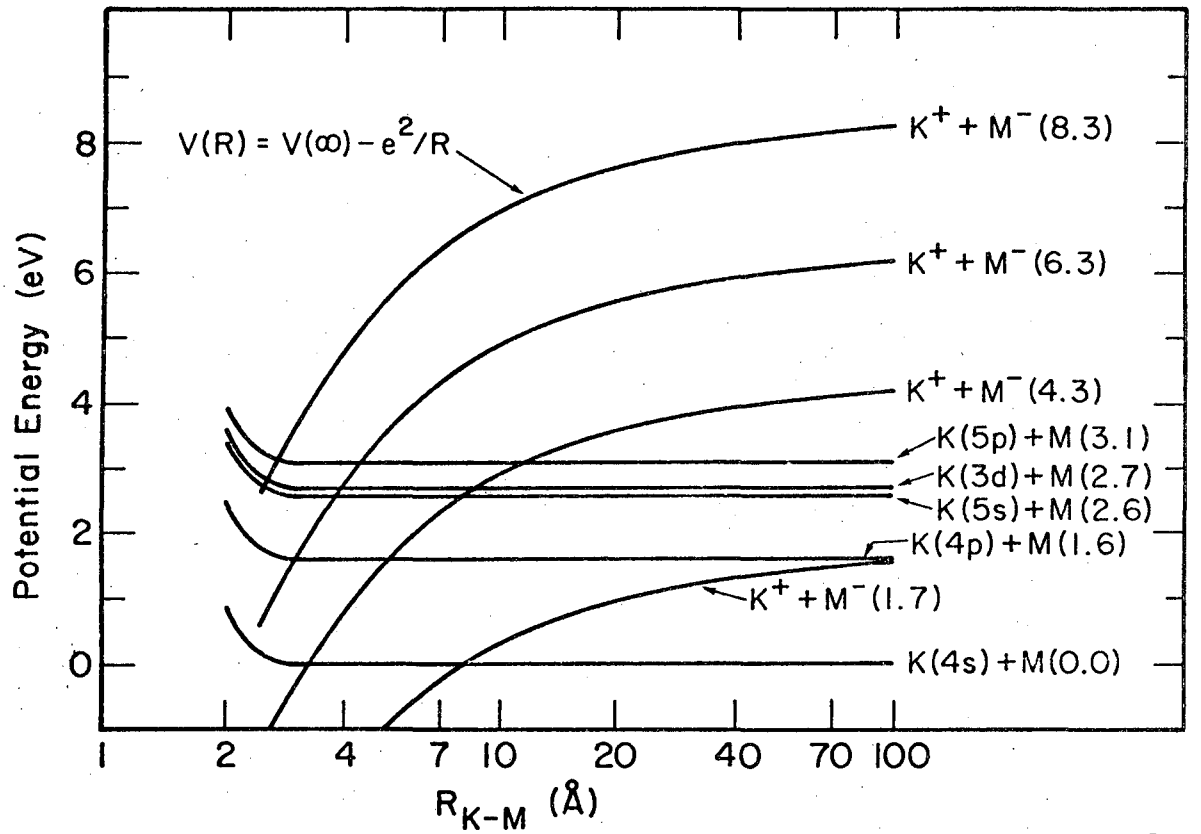

XBL 734-5999

Fig.9

LEGAL NOTICE

This report was prepared as an account of work sponsored by the United States Government. Neither the United States nor the United States Atomic Energy Commission, nor any of their employees, nor any of their contractors, subcontractors, or their employees, makes any warranty, express or implied, or assumes any legal liability or responsibility for the accuracy, completeness or usefulness of any information, apparatus, product or process disclosed, or represents that its use would not infringe privately owned rights.

TECHNICAL INFORMATION DIVISION
LAWRENCE BERKELEY LABORATORY
UNIVERSITY OF CALIFORNIA
BERKELEY, CALIFORNIA 94720